CrossMark

REGULAR PAPER

Z. Broučková · Z. Trávníček

Visualization study of hybrid synthetic jets

Abstract A synthetic jet (SJ) is a fluid flow that is created from an oscillatory process of suction and blowing. A hybrid synthetic jet (HSJ) combines this principle with fluidic pumping through a valveless pump. The present study addresses round HSJs issuing into quiescent surroundings from an actuator orifice 8 mm in diameter. For comparison purposes, a common (zero-net-mass-flux) SJ is used. The working fluid is air, and the maximum Reynolds numbers are 11,000 and 9,000 for HSJs and SJs, respectively. The following five experimental methods are employed: flow visualization using a smoke wire technique, velocity measurements using a hot-wire anemometer, velocity measurements using a Pitot tube, impedance measurements of the actuators, and measurements of the jet momentum using precision scales. Flow visualization demonstrates phase-locked flow fields. The first resonance frequencies are theoretically derived to be 79 and 98 Hz for an SJ and HSJ, respectively. These values are confirmed by all of the experimental methods used. The results demonstrate the advantages of HSJs. The tested HSJ achieves a 24 % higher pumped volume flow rate in comparison to the SJ at a maximum volumetric efficiency of 33 %. Moreover, the overall energy efficiency of the HSJ actuator is 1.8 times higher than that of the SJ actuator. These promising HSJ features, including significantly higher efficiencies, can be useful for various heat transfer applications such as the cooling of highly loaded electronic devices.

Keywords Synthetic jet · Pulsatile jet · Flow visualization · Hot-wire anemometry · Efficiency

1 Introduction

A synthetic jet (SJ) is a fluid jet flow that is created (synthesized) during an oscillatory process of suction and blowing between an SJ actuator cavity and its surroundings (Smith and Glezer 1998). The time-mean mass flux through the actuator nozzle is zero; therefore an SJ is frequently referred to as a zero-net-mass-flux jet (Cater and Soria 2002). Another term used for the same phenomenon is oscillatory vorticity generator (Yehoshua and Seifert 2006).

The first SJ actuator, to use today's terminology, was most likely the laboratory air-jet generator designed and used by Dauphinee (1957). A conference paper by Yassour et al. (1986) focused on convective heat transfer on a wall exposed to an annular impinging SJ.

The term synthetic jet was introduced by James et al. (1996). Since then, experimental, theoretical, and numerical investigations have distinctly developed (Kral et al. 1997; Mallinson et al. 2001; Lee and Goldstein 2002; Glezer and Amitay 2002; Gallas et al. 2003; Smith and Swift 2003; de Luca et al. 2014). An

Z. Broučková · Z. Trávníček (✉)
Institute of Thermomechanics, Academy of Sciences of the Czech Republic,
Dolejskova 5, 182 00 Prague 8, Czech Republic
E-mail: tr@it.cas.cz

evident reason for this fact is the relative simplicity of SJ actuators; neither blower nor fluid supply piping is required for SJ generation.

SJs are promising alternatives for various applications of active flow control such as jet vectoring (Pack and Seifert 2001; Smith and Glezer 2002), exciting (or shaking or flapping) jets (Tamburello and Amitay 2007; Ben Chiekh et al. 2011; Trávníček et al. 2012c), and flow control in external (Chen and Beeler 2002; Mittal and Rampunggoon 2002; Amitay and Glezer 2002; Tensi et al. 2002; Tang et al. 2014; Chaudhry and Zhong 2014) and internal (Ben Chiekh et al. 2003; Martin et al. 2014) aerodynamics. Another relevant field for SJ applications is heat transfer (Trávníček and Tesař 2003; Kercher et al. 2003; Mahalingam et al. 2004; Gillespie et al. 2006; Arik 2007; Valiorgue et al. 2009; Chaudhari et al. 2010; Persoons et al. 2011; Qayoum and Panigrahi 2015). Note that these SJ application possibilities increase at microscales, e.g., in micro-electromechanical systems (MEMS)—Tesař (2007). A typical microscale problem that can be effectively resolved using SJs is the cooling of highly loaded electronic components in microchannels (Timchenko et al. 2007; Lee et al. 2012a, b; Trávníček et al. 2012b). A closely related problem was studied experimentally by means of PLIF and PIV by Xia and Zhong (2012b), in which fluid mixing between two laminar water streams in a channel was enhanced by a pair of lateral SJs.

SJs can exist for given parameters provided that the fluid oscillations are strong enough to create the process of fluid jet synthesis. The problem of the SJ existence threshold is known as the SJ formation criterion (Timchenko et al. 2004; Holman et al. 2005; Shuster and Smith 2007; Zhou et al. 2009; Trávníček et al. 2012a). The closely related topic of SJ flow field regimes was investigated in recent experimental studies (Trávníček et al. 2014; McGuinn et al. 2013; Xia and Zhong 2012a).

A hybrid synthetic jet (HSJ) is a fluid jet flow produced using the same principles as those for an SJ, and also incorporates fluid pumping through the actuator cavity by means of a valveless pump [cf. the valveless pumps of Stemme and Stemme (1993), Gerlach and Wurmus (1995), and Morris and Forster (2003)]. Key elements of valveless pumps are fluidic diodes.

The fluidic diode is a fluidic element having a hydraulic resistance in one (forward) flow direction significantly smaller than that in the opposite (reverse) flow direction (Priestman and Tippetts 1985; Tesař 2007). This feature causes a fluidic diode connected to a source of symmetrical pressure oscillations to rectify oscillating flow into the forward direction. This rectification effect of the fluidic diode enhances the volume flux generation during the actuator extrusion (pump) stroke; therefore the resultant HSJ is a non-zero-net-mass-flux jet (Trávníček et al. 2005a, b, 2006, 2008; Hsu et al. 2013; Kordík and Trávníček 2013a).

Note that pulsatile fluid jets can be generated by means of different principles such as the modulation of a steady flow supply (Arwatz et al. 2008), and the modulated flows are sometimes referred to with the same expression, "hybrid synthetic jets" (Tesař et al. 2008).

The advantages and application possibilities of SJs are unquestionable. Since 2013, several types of active heat sinks for highly loaded electronic components, equipped with SJs, are commercially available. A motivation for this study is the authors' opinion that the non-zero-net-mass-flux HSJs can be a useful alternative in various applications. The advantages and application possibilities of HSJs are qualitatively the same as those mentioned for SJs. However, HSJs achieve higher volume fluxes and thus higher momentum. Therefore, HSJs can achieve more significant effects in applications of active flow control and heat transfer. Another HSJ advantage can be very useful for cooling applications; entrained fluid is taken via fluidic diodes from colder surroundings, i.e., fresh fluid without preheating can be introduced into the heat exchange zone.

2 Problem parameters

Two characteristic length scales of an axisymmetric SJ are the diameter D of the actuator output orifice and the "stroke length" $L_0 = U_0 T$, where T is the time period ($T = 1/f$, where f is frequency) and U_0 is the time-mean orifice velocity. Assuming the slug flow model, i.e., a uniform velocity profile in the actuator output orifice, U_0 is evaluated from the orifice centerline velocity at the axis ($r = 0$) (Smith and Glezer 1998):

$$U_0 = \frac{1}{T} \int_0^{T_E} u_0(r = 0, \, t) \, dt, \tag{1}$$

where T_E is the extrusion time [e.g., $T_E = T/2$ at a common sinusoidal waveform of $u_0(t)$], and u_0 is the velocity at the orifice exit ($r = 0$, $x = 0$).

The definition of the stroke length L_0 is well connected with the flow field reality and the slug flow model, because it is the length of the liquid column extruded from the cavity during the extrusion stroke of the actuation period. The dimensionless extrusion stroke length is defined as L_0/D. SJ formation for a given geometry is determined by two arbitrary dimensionless parameters from the following group: the dimensionless extrusion stroke length and the Reynolds, Stokes, and Strouhal numbers (L_0/D, Re, S, and St, respectively).

The Reynolds number is defined using the time-averaged orifice velocity during the extrusion stroke, which is $2U_0$ for a sinusoidal waveform of the velocity cycle in the orifice, $Re = 2U_0D/\nu$, where ν is the kinematic viscosity. The Strouhal number is defined in terms of the angular frequency, $\omega = 2\pi f$, as $St = \omega D/(2U_0) = \pi D/L_0$. The Stokes number is defined as $S = \sqrt{Re\,St}$. This definition can be rewritten without any additional assumptions as $S = D\sqrt{2\pi f/\nu}$, implying that the Stokes number is independent of the reference velocity. Note that the parameters Re, S, and St can be defined in many alternative ways. The present definitions are chosen to be consistent with Holman et al. (2005) and Trávníček et al. (2012a).

To quantify the overall performance of the non-zero-net-mass-flux HSJ actuators, the volumetric efficiency is defined as the ratio of the net output fluid volume extruded from the nozzle during the entire period to the total fluid volume exchanged between the actuator and its surroundings (during the same period) (Stemme and Stemme 1993; Trávníček et al. 2006). Two definitions have recently been proposed by Kordík and Trávníček (2013a). The first follows the definition by Stemme and Stemme (1993):

$$\varepsilon_V = \frac{V_P - V_S}{V_{SD} + V_S},\tag{2}$$

where V_P is the fluid volume pumped from the HSJ actuator through its nozzle during its pump stroke, V_S is the fluid volume sucked back through the same nozzle during the suction stroke, and V_{SD} is the fluid volume sucked into the HSJ actuator through the fluidic diode during the suction stroke.

The second definition is based exclusively on the volume fluxes through the HSJ actuator nozzle and does not use the volume flux through the fluidic diode (V_{SD}):

$$\varepsilon_N = \frac{V_P - V_S}{V_P + V_S}.\tag{3}$$

This is a more user-friendly definition because measurements of V_{SD} can be problematic (Kordík and Trávníček 2013a). The same definition of ε_N was used by Trávníček et al. (2006, 2008).

Two extremes of volumetric efficiency are $\varepsilon_V = \varepsilon_N = 0$ for SJ actuators and $\varepsilon_V = \varepsilon_N = 1$ for classical reciprocating pumps. Previously investigated HSJ actuators achieved $\varepsilon_N = 13\%$ Trávníček et al. (2006), 19 % Trávníček et al. (2008) and 70 % Kordík and Trávníček (2013a).

Jet momentum (for both SJs and HSJs) is generated during the extrusion stroke of the actuation period. Assuming the slug flow model, the time-average momentum flux can be evaluated by averaging over the entire period [this consideration is similar to the definition of U_0 given above by Eq. (1)]:

$$M = \frac{1}{T}\rho\left(\frac{\pi D^2}{4}\right)\int_0^{T_E} u_0^2(t)\,dt.\tag{4}$$

Assuming the slug flow model and considering harmonic actuation $u_0(t) = U_{max}\sin(\omega t)$, where U_{max} is the velocity amplitude, we can derive the time-average momentum flux as:

$$M = \rho\left(\frac{\pi D^2}{4}\right)\left(\frac{\pi U_0}{2}\right)^2.\tag{5}$$

This result will be used for evaluation of the time-mean orifice velocity U_0 from measurements of the time-mean reaction force (thrust) of the jet.

Similarly, the jet flow kinetic energy rate can be derived as

$$E = \rho\left(\frac{\pi D^2}{4}\right)\left(\frac{\pi^2}{3}\right)U_0^3.\tag{6}$$

Finally, the overall energy efficiency of the actuator can be evaluated as the ratio of the jet flow kinetic energy rate to the supply power:

$$\eta = \frac{E}{V\,I}, \tag{7}$$

where V is the supply voltage and I is the supply current (both effective values; the phase angle between V and I is negligible here). Another definition, introduced by Persoons (2012), suggests proportionality between the overall energy efficiency and the speed of sound in a fluid.

3 Experimental setup and methods

3.1 Investigated actuator

Figure 1 shows a schematic view of the actuator used in the present study, including the coordinate system x, r. The actuator was first designed and used for HSJ and SJ generation by Trávníček et al. (2006). The actuator consists of a sealed cavity equipped with a pair of electrodynamically actuating diaphragms (1) running in the opposite direction. The diaphragms of diameter $D_D = 53$ mm originate from MONACOR SP-7/4S loudspeakers with the following nominal electrical parameters: the impedance, RMS power capacity, and peak power capacity are 4 Ω, 4 W, and 8 W, respectively. The emitting orifice (2) of diameter $D = 8.0$ mm is oriented vertically upward.

Instead of a common SJ actuator design, the present actuator is equipped with a pair of fluidic diodes (3) shaped as conical ducts with apical angle $\alpha = 5.7°$, length $L_{dio} = 46$ mm, and outlet diameter $D_{dio} = 5.0$ mm. Note that the suitability of this type of diffuser/nozzle diode, known from valveless pumps (Stemme and Stemme 1993), was proved for HSJ actuators by Trávníček et al. (2005a). The forward flow direction of the conical ducts with smaller hydraulic resistance corresponds to divergent (diffuser) flow, i.e., toward the actuator cavity.

The present actuator, shown in Fig. 1, can be used for generation of either an HSJ or SJ, as follows:

- HSJ. The conical ducts are connected to the ambience.
- SJ. For comparison purposes, the conical ducts are closed and a common SJ is generated.

The working fluid is air at barometric pressure and room temperature (20–22 °C). The actuator is driven by sinusoidal current from a sweep/function generator (AGILENT 33210A). An amplifier (PIONEER A-209R) is used in this study. The range of tested frequencies is 3–300 Hz. The true RMS alternating current and voltage are measured by Metex M4660 M and Faithful FT-3900 digital multimeters, and the accuracies at all tested frequencies are ±0.8 % for both the current and voltage. In the present study the actuator was fed with sinusoidal current, and the input electrical power was kept constant at 4.0 W identically for all tested HSJs and SJs.
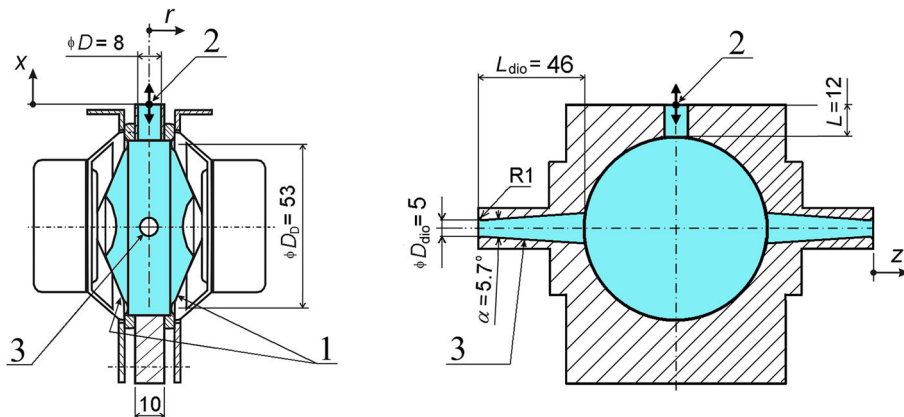

Fig. 1 Investigated actuator (sizes in mm): *1* actuating diaphragms, *2* orifice, *3* fluidic diodes shaped as conical ducts

3.2 Experimental methods

The flow visualization used the smoke wire technique. The smoke wire is made from three resistance wires 0.1 mm in diameter that are uniformly twisted together. This increases the surface area and prolongs the observation time, and the disruption of the flow is increased only slightly by the 20 % increase in hydraulic diameter. The smoke wire is located across the jet axis to be investigated, coated with liquid (Fog Fluid, DANTEC) before each test, and heated by the Joule effect of the direct electric current. White streaklines can be observed on a black background [see Trávníček and Tesař (2003) and Trávníček et al. (2012a) for more details]. The white streaklines, which trace the airflow, are traditionally referred to as ''smoke'' (in fact, the filaments consist of aerosol produced by condensation, i.e., tiny droplets of liquid).

The phase-locked flow field pattern (streaklines, diffused because of the flow turbulence) was observed under stroboscopic light (Cole Parmer 87002) synchronized with the driven frequency at an arbitrary phase angle. A device built in-house was used for adjustment of the arbitrary phase angle between the driven signal and the stroboscopic light. Pictures were taken by a digital camera connected to a PC via a USB cable using exposures ranging from 0.5 to 1.0 s. The resulting photos are multi-exposures with a large number of frames (typically, 30–100), which show the phase-locked features of the flow field while smoothing out the deviation fluctuations in the individual cycles.

Hot-wire anemometry was used to measure the velocity and quantify experimental parameters. A DANTEC MiniCTA 54T30 anemometer was used in constant temperature anemometry (CTA) mode with a single-sensor wire probe (55P16) with an NI PCI-6023E data acquisition device. The sampling frequency and the number of samples were 10 kHz and 32,768, respectively. The anemometer was calibrated over a velocity range of 0.2–43 m/s, and the linearization error of the calibration (using a four-degree polynomial) was within 8 %.

A triple decomposition process was used for the velocity analysis. The definition of the velocity components in the streamwise direction is $u = U + U_P + u'$, where $u(t)$ is the instantaneous velocity, U, U_P, and u' are the time-mean, periodic (coherent), and fluctuating (incoherent, random) components, respectively, and t/T indicates the phase during the cycle. Velocity decomposition was based on continuous sampling at a chosen frequency. For the decomposition of the CTA data, the reference sinusoidal signal from the same frequency generator was acquired in the second channel, and phase averaging was performed according to the reference signal. The phase-averaged component, $U + U_P$ (t/T), and the root mean square value, $u_{RMS}(t/T)$, indicating u' were obtained during the cycle. The number of processed periods was on the order of 10^2. Considering the reciprocating velocity characteristics at the actuator orifice, positive (extrusion) and negative (suction) flow orientations were assumed and the velocities during the suction stroke were inverted to reflect the flow direction. The data-processing procedure was scripted in MATLAB.

For demonstration purposes, the time-mean flow velocity was measured using a simple pneumometric method. In the present study, the time-mean flow velocity was measured using a Pitot tube (blunt-nosed impact tube with an outer diameter of 0.8 mm) connected to an electronic manometer (Greisinger GMH 3156 with a GMSD 2.5 MR transducer with a resolution of 0.1 Pa and an accuracy of 3 Pa). Considering the static pressure to be equal to the barometric pressure p_B, the measured time-mean total pressure p was converted into the time-mean velocity using $U = c_p[2(p–p_B)/\rho]^{0.5}$, where c_p is the pressure coefficient (approximately 1.0, in agreement with Bernoulli's equation).

It is a known fact that a Pitot tube is useful for measurements in steady flows at moderate velocity magnitudes. Obviously, the measurements cannot be applicable to pulsatile 3D flow fields in general, because they can only give reasonable results under the following conditions: the flow is non-reversing, the velocity pulsations, fluctuations, and spatial gradients are moderate, the Reynolds number is not very low, and the velocity vector direction is (at least approximately) estimable. If the velocities are too low, viscosity effects at low Reynolds numbers increase the relative errors, as analyzed in a numerical study by Boetcher and Sparrow (2007).

The present study uses a Pitot probe for simple demonstration experiments to complete indication possibilities of the resonant characteristics. The Pitot probe was always located downstream of the actuator orifice, sufficiently far from the reversing flow and large velocity pulsations, and a quantification of the local velocity was always made by CTA.

A precision scale (METTLER, Toledo, PR 8002DR) with a resolution of 0.01 g was used to measure the time-mean reaction force relating to the jet momentum. Experiments started with balancing of the actuator without any power supply with the actuator orifice oriented upward. Once the actuation began, the time-mean reaction force was measured as seeming increase of the actuator weight.

4 Results and discussion

4.1 Flow visualization

To illustrate the "jet synthesis" process of an HSJ at the driven frequency $f = 95$ Hz, Fig. 2a, b show the phase-locked presentation of the actuating period of an HSJ and the jet issuing from the conical duct (diode), respectively. The phase-locked visualizations are made for eight equal time intervals during the actuating period at a time exposure of 0.5 s. Thus, the photos are multi-exposures of 47 frames. Note that the actuator operates near the first resonance, as will be discussed theoretically and confirmed experimentally in Subsects. 4.1 and 4.2, respectively.

The period of origin ($t/T = 0$) is chosen when the extrusion stroke starts. The entire cycle consists of the extrusion and suction strokes, which are at $t/T = 0-T_E/T$ and $T_E/T-1$, respectively. Note that T_E/T of the present HSJ is larger than 0.5 (i.e., value for an ideal SJ cycle). A hot-wire-based quantifications of T_E/T for HSJ and SJ are discussed below.

The main feature, visible in the sequence of photographs in Fig. 2a, is the generated fluid "puff", i.e., the large vortex structure passing downstream of the observation area. The extrusion of fluid through the orifice and the formation of the large vortex structure near the orifice are clearly visible for $t/T = 0.125$–0.5 in Fig. 2a.

Later, for $t/T = 0.625$–1, the actuator operates in the suction stroke ingesting the external fluid. The inertia of the large vortex structure results in it moving downstream independently of the local situation in the orifice, where the flow orientation is reversed into the actuator cavity. Note that the ranges of the actuator suction, i.e., saddle points on the jet axis, were revealed by means of CTA measurements at $x/D = 1.1$ for an SJ at 75 Hz and $x/D = 0.9$ for an HSJ at 95 Hz (Trávníček et al. 2006). Finally, at $t/T = 1$, the whole cycle is repeated.

The behavior of the jet issuing from the conical duct (diode), shown in Fig. 2b, is similar to that described for the HSJ in Fig. 2a. Obviously, the qualitative visualization cannot clearly register a fluidic
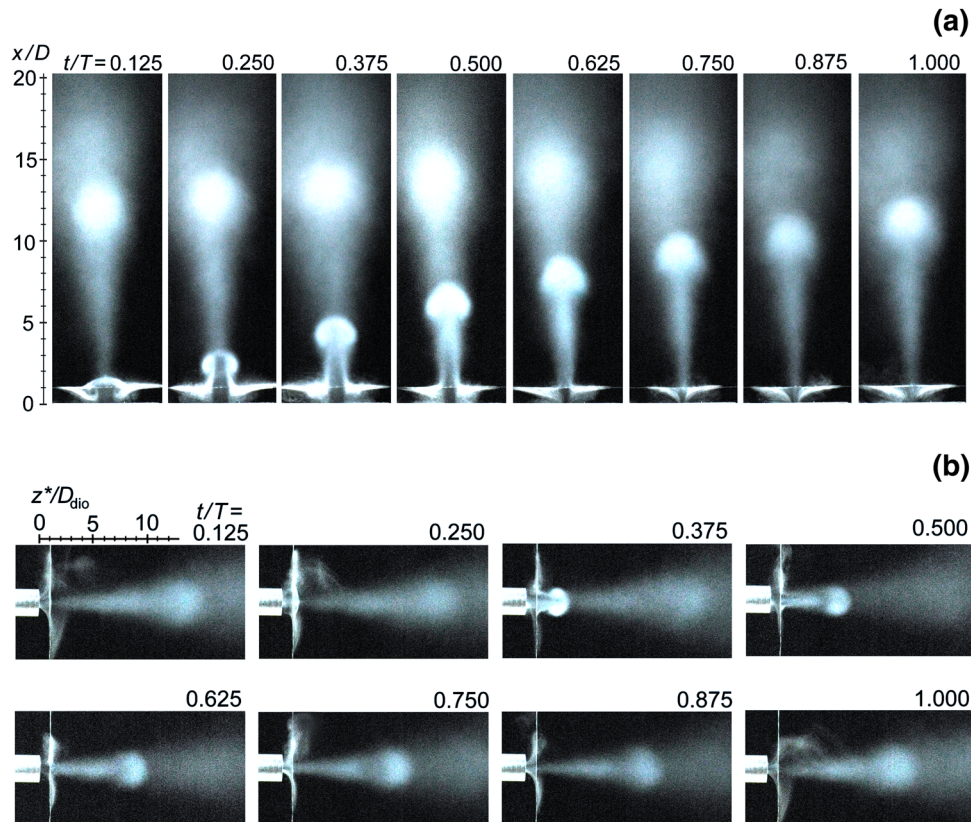

Fig. 2 Phase-locked flow visualization during the actuating cycle at $f = 95$ Hz. **a** HSJ, **b** jet issuing from conical duct (diode)

diode particularity associated with its rectification effect. A quantification of this effect is made by means of CTA measurements, and the results obtained are described in the following subsection.

4.2 Resonance behavior

To analyze the resonance behavior of the actuators, we use a basic mechanical model similarly to Trávníček et al. (2005a). This model is sufficient to find the first resonance, which is of interest in the present study. More complex models have recently been proposed, including a theoretical derivation supported by experimental validation revealing higher-order resonances (up to fifth order) by Kordík and Trávníček (2013b).

In the following text, the resonance behavior of the present actuator, shown in Fig. 1, is described for generating either SJs or HSJs, i.e., the conical ducts are either closed or opened, respectively.

An SJ is generated when the actuator conical ducts are closed. Considering fluid incompressibility, the potential energy of the pair of diaphragms is transformed into the kinetic energy of the fluid during each period. The potential energy of the rigid, piston-like diaphragms can be written in terms of the energy of linear springs. If the steady overpressure p causes a steady displacement Δy of the diaphragm, the diaphragm spring constant is defined as $K_P = p/\Delta y$.

The kinetic energy of an SJ is assumed to be captured in a fluid column of effective length L_e, where $L_e = L + 8D/(3\pi)$ and L is the orifice length—see Kinsler et al. (2000). Following the derivation described in Trávníček et al. (2005a), the first natural frequency of the actuator-generated SJ can be derived as.

$$f_{SJ} = \frac{1}{2\pi}\left(\frac{D}{D_D}\right)\sqrt{\frac{K_P}{2\rho L_e}}, \tag{8}$$

where ρ is the fluid (air) density and K_P was evaluated by an auxiliary experiment for the present diaphragms as $K_P = 4.8 \times 10^5$ N/m^3. For the geometry (Fig. 1) and parameters of this study ($\rho = 1.177$ kg/m^3), Eq. (8) yields a frequency $f_{SJ} = 79$ Hz.

An HSJ is generated by the actuator shown in Fig. 1 when its conical ducts are connected with the ambience and operate as fluidic diodes. The derivation of the first natural frequency is similar to Eq. (8) for the case of an SJ. While the evaluation of the potential energy is the same, the fluid kinetic energy has two contributions, namely the kinetic energy of the HSJ plus the kinetic energy of the fluid flowing through the pair of fluidic diodes. Assuming identical maximum outlet velocities from the nozzle and diode during the pump stroke, the first natural frequency of the actuator generated HSJ can be derived as

$$f_{HSJ} = \frac{1}{2\pi}\left(\frac{D^2 + 2D_{dio}^2}{D_D}\right)\sqrt{\frac{K_P}{2\rho\left[L_e D^2 + \frac{2D_{dio}^4}{\tan(\alpha)}\left(\frac{1}{D_{dio}} - \frac{1}{D_{dio}+\tan(\alpha)L_{dio,e}}\right)\right]}}, \tag{9}$$

where D_{dio} is the outlet (smaller) diameter of the diodes, α is the tangent of the apex angle of the diode cone, and $L_{dio,e}$ is the equivalent fluid column length of the diode. In this study, $L_{dio,e}$ is estimated as $L_{dio,e} = L_{dio} + 8D_{dio}/(3\pi)$, where L_{dio} is the length of the diode cone—see Fig. 1. This estimation, based on the case of a simple orifice, neglects any alteration of the equivalent fluid column lengths during the suction and pump strokes, resulting in a slight alteration of the natural frequencies (cf. Trávníček et al. 2005a). For the actuator geometry (Fig. 1) and parameters of this study ($\rho = 1.177$ kg/m^3), Eq. (9) yields a frequency $f_{HSJ} = 98$ Hz. The previously mentioned negligible alteration of f_{HSJ} during the suction and pump strokes is estimated to be less than 2 %.

It is worthy of notice here that the limiting case of a very small diode, $D_{dio} \to 0$, causes Eq. (9) to be transformed into Eq. (8). This is obvious because the HSJ actuator without fluidic diodes becomes the SJ actuator described above.

4.3 Frequency characteristics

The velocity resonance curve (the dependence of the velocity amplitude on the driving frequency) is evaluated experimentally at a constant power input, similarly to previous studies (Trávníček et al. 2005a, 2006).

Figure 3a shows the time-mean orifice velocity U_0 evaluated from the CTA measurement of the orifice centerline velocity of the SJ and HSJ—see HSJ (CTA) and SJ (CTA) curves. The maxima of both curves
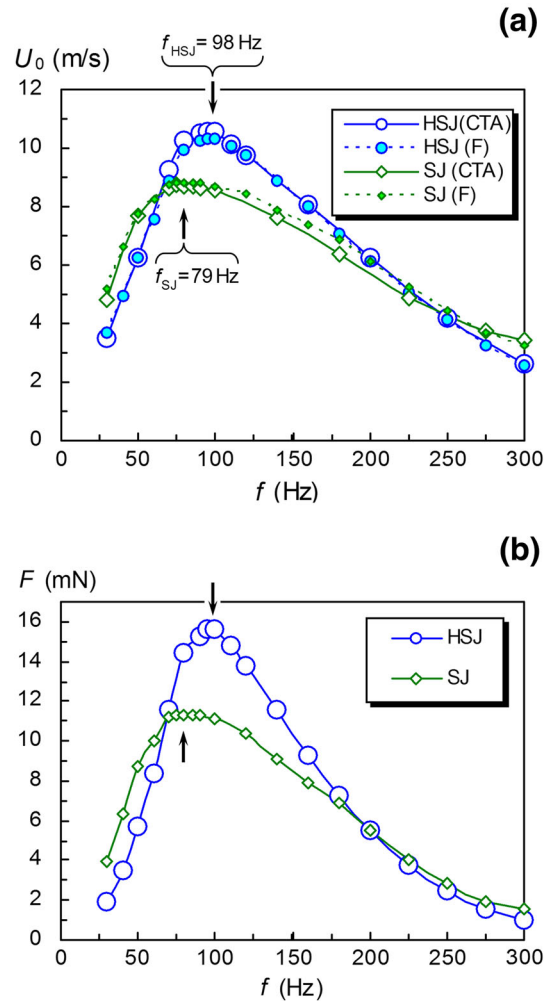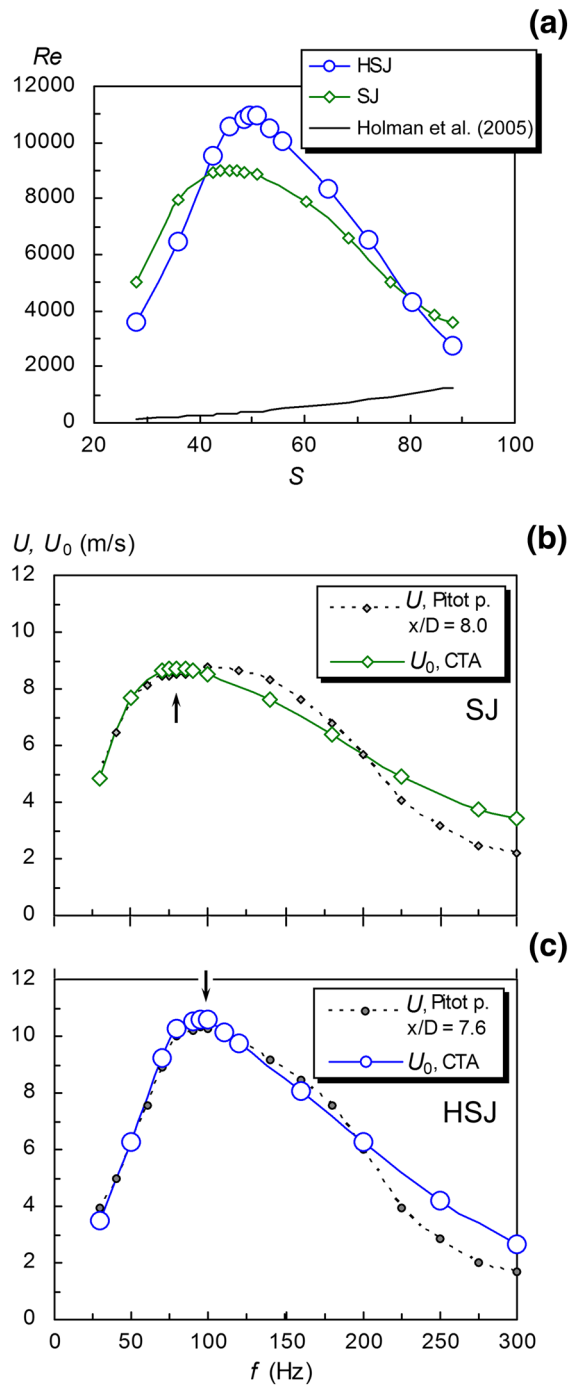
Fig. 3 Frequency characteristics for the SJ and HSJ. **a** Velocity resonance curves—comparison of the CTA measurements with U_0 evaluated from the reaction force (F), **b** reaction forces measured using precision scales

clearly indicate the first resonances. Obviously, these maxima are in a good agreement with the theoretical values of $f_{SJ} = 79$ Hz and $f_{HSJ} = 98$ Hz predicted by Eqs. (8) and (9), respectively (the arrows in Figs. 3, 4, 5 graphically indicate the theoretical values). These results confirm the previous findings for the same actuator acquired by a different CTA system—see Trávníček et al. (2006). In the following text, several alternative experimental approaches useful for obtaining the first resonance are presented.

Figure 3b shows the time-mean reaction forces relating to the jet momentum (jet thrust) measured using precision scales for the SJ and HSJ. The maxima of the experimental curves demonstrate the first resonances, which are very close to the theoretical values indicated by the arrows. Using the time-average momentum given by Eq. (5), the values were transformed into U_0 velocity data. Figure 3a compares the resultant U_0 velocities evaluated from the momentum with the CTA data discussed above—see HSJ (F) and SJ (F) curves. Evidently, the U_0 velocities obtained from the measurement of the reaction forces are in a good agreement with the CTA data—the differences are within 7.5 %. Note that this agreement cannot be generalized as yet because it is only valid for the present geometry and parameter ranges.

The visualization results clearly demonstrate that fluid oscillations from the actuators investigated for the given parameters are strong enough to create fluid jets—e.g., Fig. 2a. To present this fact quantitatively, the CTA data from Fig. 3a are transformed into a dimensionless form of the Reynolds and Stokes numbers, as shown in Fig. 4a. The maximum Reynolds numbers were approximately $Re = 9{,}000$ and $11{,}000$ for the SJ and HSJ, respectively.

Fig. 4 Frequency characteristics for the SJ and HSJ: velocity resonance curves evaluated by **a** CTA in dimensionless form, including a comparison with the SJ existence threshold of Holman et al. (2005), **b** Pitot probe experiments for the SJ, **c** Pitot probe experiments for the HSJ

The threshold of SJ existence, $Re = 0.16\ S^2$ according to Holman et al. (2005), is plotted in Fig. 4a. Evidently, all the present data are significantly above this threshold. For the resonance frequencies (79 and 98 Hz for the SJ and HSJ, respectively), the present data are one order above the threshold. Even at the upper end of the frequency range investigated, $f = 300$ Hz, the present data are more than double the threshold.
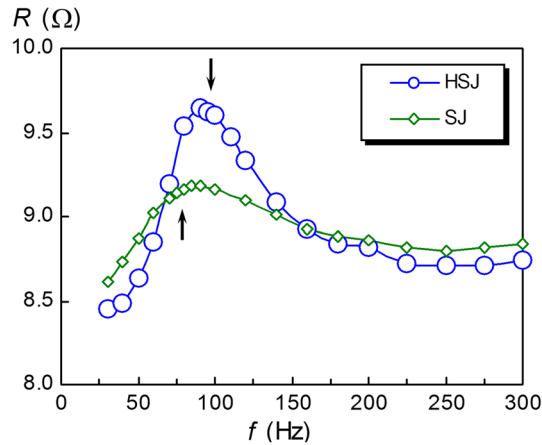
Fig. 5 Frequency characteristics for the SJ and HSJ presented in terms of electrical impedance

Another method available for finding the resonance frequencies is Pitot tube utilization. Figures 4b and c show the velocity resonance curves of the SJ and HSJ, respectively. For comparison purposes, the U_0 velocities measured by CTA are also plotted. The maxima of the Pitot tube data agree well with the first resonances revealed by the CTA data as well as with the theoretical derivations indicated by the arrows. It is fair to say that the drawback of this method is the necessary predetermination of the Pitot tube location obeying the condition of $U = U_0$, where the velocity U is measured by the Pitot probe and the velocity U_0 is evaluated from the CTA data. The probe location was $x/D = 8.0$ for the SJ in Fig. 4b and $x/D = 7.6$ for the HSJ in Fig. 4c.

In the present case of the electrodynamically driven actuator, the resonance frequency can be easily indicated by measuring the electrical impedance—see Greco et al. (2013). The impedance R was evaluated as the ratio of the voltage to the current, both in effective values, $R = V/I$ (the phase angle is negligible here). The results are shown in Fig. 5. Once again, the maxima of the experimental curves indicate the first resonances, which are very close to the theoretical values indicated by the arrows.
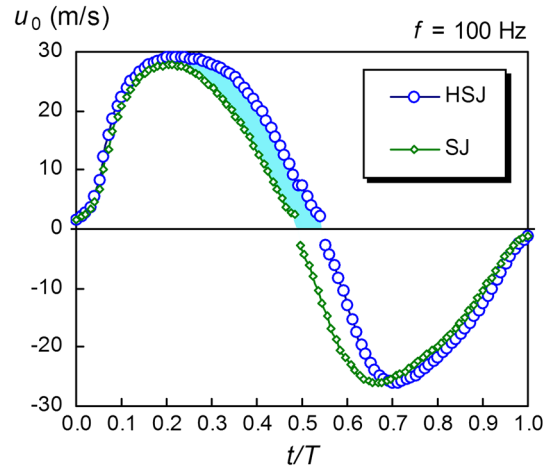
4.4 Flow velocity cycles

The centerline velocity cycles of the HSJ and SJ were measured at $x = 0$, $r = 0$, and the resulting (phase-averaged) cycles at $f = 100$ Hz are shown in Fig. 6. While the nearly sinusoidal character of the SJ velocity cycle is obvious, the HSJ has a distinctly longer extrusion stroke, $T_E/T = 0.55$ (on the contrary, the extrusion time of SJ is slightly shorter than the half-period, $T_E/T = 0.49$). Integration of the velocity cycles according to Eq. (1) gives the time-mean orifice velocities $U_0 = 10.6$ and 8.5 m/s for the HSJ and SJ, respectively. Thus, the value of the pump volume flow rate for the HSJ is 24 % higher. This enhancement is depicted as a colored area in Fig. 6. It is partly caused by the increase of the pump velocity maximum (by 5 %), but mainly by an asymmetry of the extrusion–suction strokes in time with an extended HSJ extrusion stroke. Note that these velocities agree very well with previous measurements performed with the same actuator at slightly different frequencies (75 and 95 Hz for an SJ and HSJ, respectively) with a different CTA system—see Trávníček et al. (2006)—the differences in velocities are within 4 %; the previous velocities were slightly higher.

4.5 Volumetric and energy efficiencies

Figure 7a presents an evaluation of the volumetric efficiency ε_N from CTA data using Eq. (3). According to the explanation in Sect. 2, ε_N must be zero for SJs. Despite the values shown in Fig. 7a being nonzero, they are acceptably small—less than 4 % except for the first point of 6.5 %.

This is caused partly by experimental uncertainty, but mainly by a simplification incorporated in the adopted slug flow model. In other words, the velocity measurements were made along the jet axis only. Acceptably small values in Fig. 7a can be considered a validation of the slug flow model for the present geometry and range of parameters.

Fig. 6 Centerline velocity cycles of the HSJ and SJ measured at $x = 0$, $r = 0$
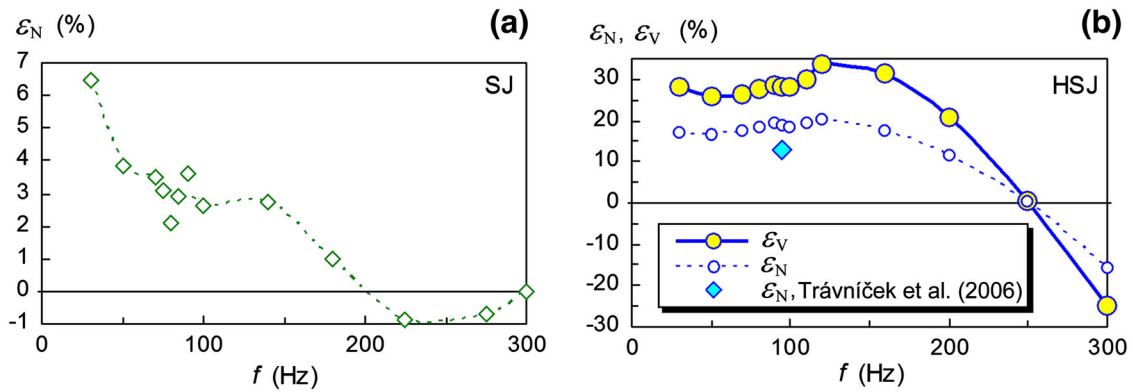
Fig. 7 Evaluation of the volumetric efficiencies from CTA data. **a** Validation of the present model and methods by means of the SJ, **b** volumetric efficiencies of the HSJ

Figure 7b shows the volumetric efficiencies ε_N and ε_V of the HSJ. The maximum values achieved are 20 and 33 %, respectively. For comparison purposes, a data point indicating ε_N evaluated at 95 Hz by Tráv-níček et al. (2006) is also plotted. This point is located 5.5 % below the ε_N curve of the present study. Note that this point was obtained without the slug flow model, and the volume fluxes were evaluated by integration of the velocity profiles. The comparison in Fig. 7b indicates, similarly to Fig. 7a, that the present slug flow model causes a small overprediction of the true ε_N values. Finally, the less than 5 % differences advocate reasonably well the applicability of the slug flow model based on CTA point measurements for the present geometry and parameter ranges.

A comparably small overprediction can be considered for the ε_V values. However, there is no available comparison of ε_V values obtained without the slug flow model, because an evaluation of the volume fluxes through the fluidic diode (having a small diameter and rounded edges) is highly problematic.

Finally, the jet flow kinetic energy rate and the overall energy efficiency can be evaluated from Eqs. 6 and 7. Obviously, the maximum performance is achieved at the resonance frequencies of $f_{SJ} = 79$ Hz and $f_{HSJ} = 98$ Hz. For these frequencies, the maximum efficiencies of the SJ and HSJ actuators are $\eta = 3.2$ and 5.8 %. It is worth noting here that a relatively low level of both η values results from an adaptation of the electrodynamic acoustic driver (loudspeaker) for the present investigation. Obviously, the loudspeaker design aims at undistorted acoustic performance over a wide frequency range without any requirements on the energy efficiency. Therefore, the relation between these values can be considered more important than the actual values, namely the fact that the HSJ actuator achieves a 1.8 times higher overall energy efficiency than the SJ actuator. This evaluation is another quantification of the advantages of HSJs over common SJs.

5 Conclusions

Two pulsatile round air jets were experimentally tested, namely, the common zero-net-mass-flux synthetic jet (SJ) and the non-zero-net-mass-flux hybrid synthetic jet (HSJ). The proper function of the actuator was confirmed experimentally using the following five methods: flow visualization using a smoke wire technique, velocity measurements using a hot-wire anemometer, velocity measurements using a Pitot tube, impedance measurements of the actuators, and measurements of the time-mean reaction force relating to the jet momentum using precision scales.

The first resonance frequencies were derived theoretically for both the SJ and HSJ. The experiments confirmed the theoretically predicted values of $f_{SJ} = 79$ Hz and $f_{HSJ} = 98$ Hz. The Reynolds numbers achieved were 9,000 and 11,000 for the SJ and HSJ, respectively. The applicability of the slug flow model based on CTA point measurements for the present geometry and parameter ranges was confirmed.

The results demonstrate the advantages of HSJs. The HSJ achieves a 24 % higher pumped volume flow rate in comparison with the common SJ. The maximum volumetric efficiencies ε_N and ε_V are 20 and 33 %, respectively. The overall energy efficiencies of the SJ and HSJ actuators are evaluated to be $\eta = 3.2$ and 5.8 %, respectively. This means that the HSJ actuator achieves a 1.8 times higher overall energy efficiency than the SJ actuator. These promising HSJ features can be useful for various heat transfer applications such as the cooling of highly loaded electronic devices.

References

Amitay M, Glezer A (2002) Controlled transients of flow reattachment over stalled airfoils. Int J Heat Fluid Flow 23:690–699

Arik M (2007) An investigation into feasibility of impingement heat transfer and acoustic abatement of meso scale synthetic jets. Appl Therm Eng 27:1483–1494

Arwatz G, Fono I, Seifert A (2008) Suction and oscillatory blowing actuator modeling and validation. AIAA J 46:1107–1117

Ben Chiekh M, Bera JC, Sunyach M (2003) Synthetic jet control for flows in a diffuser: vectoring, spreading and mixing enhancement. J Turbul 4:1–12

Ben Chiekh M, Ferchichi M, Bera J-C (2011) Modified flapping jet for increased jet spreading using synthetic jets. Int J Heat Fluid Flow 32:865–875

Boetcher SKS, Sparrow EM (2007) Limitations of the standard Bernoulli equation method for evaluating Pitot/impact tube data. Int J Heat Mass Transf 50:782–788

Cater JE, Soria J (2002) The evolution of round zero-net-mass-flux jets. J Fluid Mech 472:167–200

Chaudhari M, Puranik B, Agrawal A (2010) Heat transfer characteristics of synthetic jet impingement cooling. Int J Heat Mass Transf 53:1057–1069

Chaudhry IA, Zhong S (2014) A single circular synthetic jet issued into turbulent boundary layer. J Vis 17:101–111

Chen F-J, Beeler GB (2002) Virtual shaping of a two-dimensional NACA 0015 airfoil using synthetic jet actuator. AIAA Paper 2002–3273

Dauphinee TM (1957) Acoustic air pump. Ref Sci Instrum 28:456

de Luca L, Girfoglio M, Coppola G (2014) Modeling and experimental validation of the frequency response of synthetic jet actuators. AIAA J 52:1733–1748

Gallas Q, Holman R, Nishida T, Carroll B, Sheplak M, Cattafesta L (2003) Lumped element modeling of piezoelectric-driven synthetic jet actuators. AIAA J 41:240–247

Gerlach T, Wurmus H (1995) Working principle and performance of the dynamic micropump. Sens Actuator A-Phys 50:135–140

Gillespie MB, Black WZ, Rinehart C, Glezer A (2006) Local convective heat transfer from a constant heat flux flat plate cooled by synthetic air jets. J Heat Transf-Trans ASME 128:990–1000

Glezer A, Amitay M (2002) Synthetic jets. Annu Rev Fluid Mech 34:503–529

Greco CS, Ianiro A, Astarita T, Cardone G (2013) On the near field of single and twin circular synthetic air jets. Int J Heat Fluid Flow 44:41–52

Holman R, Utturkar Y, Mittal R, Smith BL, Cattafesta L (2005) Formation criterion for synthetic jets. AIAA J 43:2110–2116

Hsu S-S, Trávníček Z, Chou C-C, Chen C-C, Wang A-B (2013) Comparison of double-acting and single-acting synthetic jets. Sens Actuator A-Phys 203:291–299

James RD, Jacobs JW, Glezer A (1996) A round turbulent jet produced by an oscillating diaphragm. Phys Fluids 8:2484–2495

Kercher DS, Lee J-B, Brand O, Allen MG, Glezer A (2003) Microjet cooling devices for thermal management of electronics. IEEE Trans Compon Pack Manuf Technol 26:359–366

Kinsler LE, Frey AR, Coppens AB, Sanders JV (2000) Fundamentals of acoustics, 4th edn. Wiley, New York, pp 184–187

Kordík J, Trávníček Z (2013a) Axisymmetric synthetic jet actuators with large streamwise dimensions. AIAA J 51:2862–2877

Kordík J, Trávníček Z (2013b) Novel fluidic diode for hybrid synthetic jet actuator. J Fluids Eng-Trans ASME 135:101101-1–101101-7

Kral LD, Donovan JF, Cain AB, Cary AW (1997) Numerical simulation of synthetic jet actuators. AIAA Paper 97–1824

Lee CY, Goldstein DB (2002) Two-dimensional synthetic jet simulation. AIAA J 40:510–516

Lee A, Timchenko V, Yeoh GH, Reizes JA (2012a) Three-dimensional modelling of fluid flow and heat transfer in micro-channels with synthetic jet. Int J Heat Mass Transf 55:198–213 (Erratum (2012) in Int J Heat Mass Transf 55:2746)

Lee A, Yeoh GH, Timchenko V, Reizes JA (2012b) Flow structure generated by two synthetic jets in a channel: effect of phase and frequency. Sens Actuator A-Phys 184:98–111

Mahalingam R, Rumigny N, Glezer A (2004) Thermal management using synthetic jet ejectors. IEEE Trans Compon Pack Technol 27:439–444

Mallinson SG, Reizes A, Hong G (2001) An experimental and numerical study of synthetic jet flow. Aeronaut J 105:41–49

Martin ND, Bottomley M, Packwood A (2014) Switching of a bi-stable diverter valve with synthetic jet actuators. AIAA J 52:1563–1567

McGuinn A, Farrelly R, Persoons T, Murray DB (2013) Flow regime characterisation of an impinging axisymmetric synthetic jet. Exp Therm Fluid Sci 47:241–251

Mittal R, Rampunggoon P (2002) On the virtual aeroshaping effect of synthetic jets. Phys Fluids 14:1533–1536

Morris CJ, Forster FK (2003) Low-order modeling of resonance for fixed-valve micropumps based on first principles. J Microelectromech Syst 12:325–334

Pack LG, Seifert A (2001) Periodic excitation for jet vectoring and enhanced spreading. J Aircr 38:486–495

Persoons T (2012) General reduced-order model to design and operate synthetic jet actuators. AIAA J 50:916–927

Persoons T, McGuinn A, Murray DB (2011) A general correlation for the stagnation point Nusselt number of an axisymmetric impinging synthetic jet. Int J Heat Mass Transf 54:3900–3908

Priestman GH, Tippetts JR (1985) Factors affecting the application of vortex diodes and throttles. In: Proceedings of Symposium fluid control and measurement (FLUCOME), Pergamon, pp 241–246, Oxford

Qayoum A, Panigrahi PK (2015) Synthetic jet interaction with approaching turbulent boundary layer for heat transfer enhancement. Heat Transf Eng 36:352–367

Shuster JM, Smith DR (2007) Experimental study of the formation and scaling of a round synthetic jet. Phys Fluids 19:045109-1–045109-21

Smith BL, Glezer A (1998) The formation and evolution of synthetic jets. Phys Fluids 10:2281–2297

Smith BL, Glezer A (2002) Jet vectoring using synthetic jets. J Fluid Mech 458:1–34

Smith BL, Swift GW (2003) A comparison between synthetic jets and continuous jets. Exp Fluids 34:467–472

Stemme E, Stemme G (1993) A valve-less diffuser/nozzle-based pump. Sens Actuator A-Phys 39:159–167

Tamburello DA, Amitay M (2007) Three-dimensional interactions of a free jet with a perpendicular synthetic jet. J Turbul 8:1–18

Tang H, Salunkhe P, Zheng YY, Du JX, Wu YH (2014) On the use of synthetic jet actuator arrays for active flow separation control. Exp Therm Fluid Sci 57:1–10

Tensi J, Boué I, Paillé F, Dury G (2002) Modification of the wake behind a circular cylinder by using synthetic jets. J Vis 5:37–44

Tesař V (2007) Pressure-driven microfluidics. Artech house integrated microsystems. Artech House Publishers, Boston

Tesař V, Trávníček Z, Kordík J, Randa Z (2008) Experimental investigation of a fluidic actuator generating hybrid-synthetic jets. Sens Actuator A-Phys 138:213–220

Timchenko V, Reizes J, Leonardi E, de Vahl Davis G (2004) A criterion for the formation of micro synthetic jets. In: Proceedings of IMECE04, IMECE2004-61374 260:197–203, New York

Timchenko V, Reizes JA, Leonardi E (2007) An evaluation of synthetic jets for heat transfer enhancement in air cooled micro-channels. Int J Numer Methods Heat Fluid Flow 17:263–283

Trávníček Z, Tesař V (2003) Annular synthetic jet used for impinging flow mass–transfer. Int J Heat Mass Transf 46:3291–3297

Trávníček Z, Fedorchenko AI, Wang A-B (2005a) Enhancement of synthetic jets by means of an integrated valve-less pump, Part I: design of the actuator. Sens Actuator A-Phys 120:232–240

Trávníček Z, Tesař V, Wang A-B (2005b) Enhancement of synthetic jets by means of an integrated valve-less pump, Part II: numerical and experimental studies. Sens Actuator A-Phys 125:50–58

Trávníček Z, Vít T, Tesař V (2006) Hybrid synthetic jet as the non-zero-net-mass-flux jet. Phys Fluids 18:081701-1–081701-4

Trávníček Z, Tesař V, Kordík J (2008) Performance of synthetic jet actuators based on hybrid and double-acting principles. J Vis 11:221–229

Trávníček Z, Broučková Z, Kordík J (2012a) Formation criterion for axisymmetric synthetic jets at high Stokes numbers. AIAA J 50:2012–2017

Trávníček Z, Dančová P, Kordík J, Vít T, Pavelka M (2012b) Heat and mass transfer caused by a laminar channel flow equipped with a synthetic jet array. Trans ASME J Therm Sci Eng Appl 2:041006-1–041006-8

Trávníček Z, Němcová L, Kordík J, Tesař V, Kopecký V (2012c) Axisymmetric impinging jet excited by a synthetic jet system. Int J Heat Mass Transf 55:1279–1290

Trávníček Z, Broučková J, Kordík J (2014) Visualization of synthetic jet formation in air. J Vis (in review)

Valiorgue P, Persoons T, McGuinn A, Murray DB (2009) Heat transfer mechanisms in an impinging synthetic jet for a small jet-to-surface spacing. Exp Therm Fluid Sci 33:597–603

Xia Q, Zhong S (2012a) An experimental study on the behaviours of circular synthetic jets at low Reynolds numbers. Proc Inst Mech Eng Part C-J Eng Mech Eng Sci 226:2686–2700

Xia Q, Zhong S (2012b) A PLIF and PIV study of liquid mixing enhanced by a lateral synthetic jet pair. Int J Heat Fluid Flow 37:64–73

Yassour Y, Stricker J, Wolfshtein M (1986) Heat transfer from a small pulsating jet. In: Proceedings of 8th International Heat Transfer Conference 3:1183–1186, San Francisco

Yehoshua T, Seifert A (2006) Boundary condition effects on the evolution of a train of vortex pairs in still air. Aeronaut J 110:397–417

Zhou J, Tang H, Zhong S (2009) Vortex roll-up criterion for synthetic jets. AIAA J 47:1252–1262